

Characterizing damage zones of normal faults using seismic variance in the Wangxuzhuang oilfield, China

Zonghu Liao¹, Luyao Hu², Xiaodi Huang³, Brett M. Carpenter⁴, Kurt J. Marfurt⁴, Saiynna Vasileva², and Yun Zhou²

Abstract

We have investigated the distribution and thickness of damage zones for a system of secondary normal faults in the subsurface of the Wangxuzhuang oilfield, China. Based on seismic variance analysis, we find (1) four isolated faults with approximately 2 km length and approximately 200 m damage-zone thickness. The damage zones of these isolated faults reveal a decaying intensity of deformation from the fault core to the protolith, which fits a power-law form $y = ax^{-b}$ similar to that observed in the field. (2) A merged fault with approximately 400 m thickness. (3) A bifurcated fault with approximately 400 m thickness and three linked segments. Damage zones that consist of several subsidiary faults are thicker than those of isolated faults. The displacement-length analyses of the four isolated faults suggest the constant-length growth of the limestone in this case. We determine the potential to apply seismic variance to systematically characterize damage zones as potential fluid migration conduits on the basin scale.

Introduction

Fault zones are commonly described to consist of a fault core and surrounding damage zone, which differs structurally, mechanically, and hydrologically from the undeformed host rock (protolith) (Chester and Logan, 1986; Caine et al., 1996; Sagy et al., 2001; Katz et al., 2003; Savage and Brodsky, 2011). The damage zone, with structures that formed as a result of the faulting process, likely consists of complex fracture networks, owing to fault-related diagenesis, segmentation, and evolution (Laubach et al., 2014). With limited data and access, it is challenging to evaluate the structure of damage zones in the subsurface and to determine how the damage zone affects the migration, accumulation, and leakage of subsurface fluids (Caine et al., 1996; Faulkner et al., 2010; Busetti et al., 2012; Ellis et al., 2012).

Previous quantitative methods for characterizing fault damage zones have been based on measured fracture density, seismic event data, and geophysical logging data. (1) Using outcrop measurements to map the fracture density as a function of distance from the fault core. The damage-zone thickness of the fault is found by determining the distance at which the damage falls below the background level on both sides of the fault (Vermilye

and Scholz, 1998; Mitchell and Faulkner, 2009). (2) Via analysis of the density and distribution of seismic events recorded during the 1992 Landers earthquake in California, the damage zone width was roughly estimated (Peng et al., 2003). (3) Zoback et al. (2011) interpret structural characteristics of the San Andreas Fault zone using borehole logging methods. The damage zone of the fault was identified by identifying a reduction in V_p and V_s . Although these three methods are widely accepted, particularly for isolated fault strands, they lack feasibility and proper resolution for characterizing faults in the subsurface on the basin scale. Such faults have been shown to significantly impact reservoir connectivity and petroleum migration (Faulkner et al., 2010; Rossetti et al., 2010; Yan et al., 2016).

With the advantages of seismic surveys, the detection of fault zones in the subsurface can be done indirectly by using seismic analyses, including seismic simulation (Botter et al., 2016) and seismic attributes (Iacopini and Butler, 2011). Seismic attributes such as azimuth, dip, and coherence, can not only be used to enhance the recognition of a fault network, but also to characterize the fault zone architecture and properties (Chopra and Marfurt, 2007; Botter et al., 2016; Liao et al., 2017). The

¹China University of Petroleum (Beijing), State Key Laboratory of Petroleum Resources and Prospecting, Beijing 102249, China and China University of Petroleum (Beijing), College of Geosciences, Beijing 102249, China. E-mail: zonghuliao@163.com (corresponding author).

²China University of Petroleum (Beijing), College of Geosciences, Beijing 102249, China. E-mail: hulyao1993@foxmail.com; sainavas@mail.ru; zhouyun_zoe@163.com.

³PetroChina Dagang Oilfield Company, CNPC, Second Oil Production Plant, Tianjin 300280, China. E-mail: 554545516@qq.com.

⁴University of Oklahoma, School of Geosciences, Norman, Oklahoma 73019, USA. E-mail: brett.carpenter@ou.edu; kmarfurt@ou.edu.

Manuscript received by the Editor 8 January 2020; revised manuscript received 26 March 2020; published ahead of production 30 April 2020. This paper appears in *Interpretation*, Vol. 8, No. 4 (November 2020); p. 1–8, 7 FIGS., 1 TABLE.

<http://dx.doi.org/10.1190/INT-2020-0004.1>. © 2020 Society of Exploration Geophysicists and American Association of Petroleum Geologists. All rights reserved.

attribute of seismic coherence measures changes in the waveform from the seismic reflection and provides a potential quantitative measure of damage-zone thickness. This approach has been used to analyze the wide damage zone of a 20 km strike-slip fault in Oklahoma's subsurface (Liao et al., 2019). It has been demonstrated that this approach can reveal the dimensions and shapes of damage zones with some indications of the intensity of its deformation. However, the seismic expression of fault damage is usually combined with seismic noise and unknown complex features from the fault itself. With the exception of a few cases, it is challenging to obtain a realistic, conceptual understanding of the fault system in the subsurface. In this study, we apply the seismic attribute of variance (Pigott et al., 2013; Liao et al., 2017) to describe a system of small secondary normal faults in the Wangxuzhuang Basin, China.

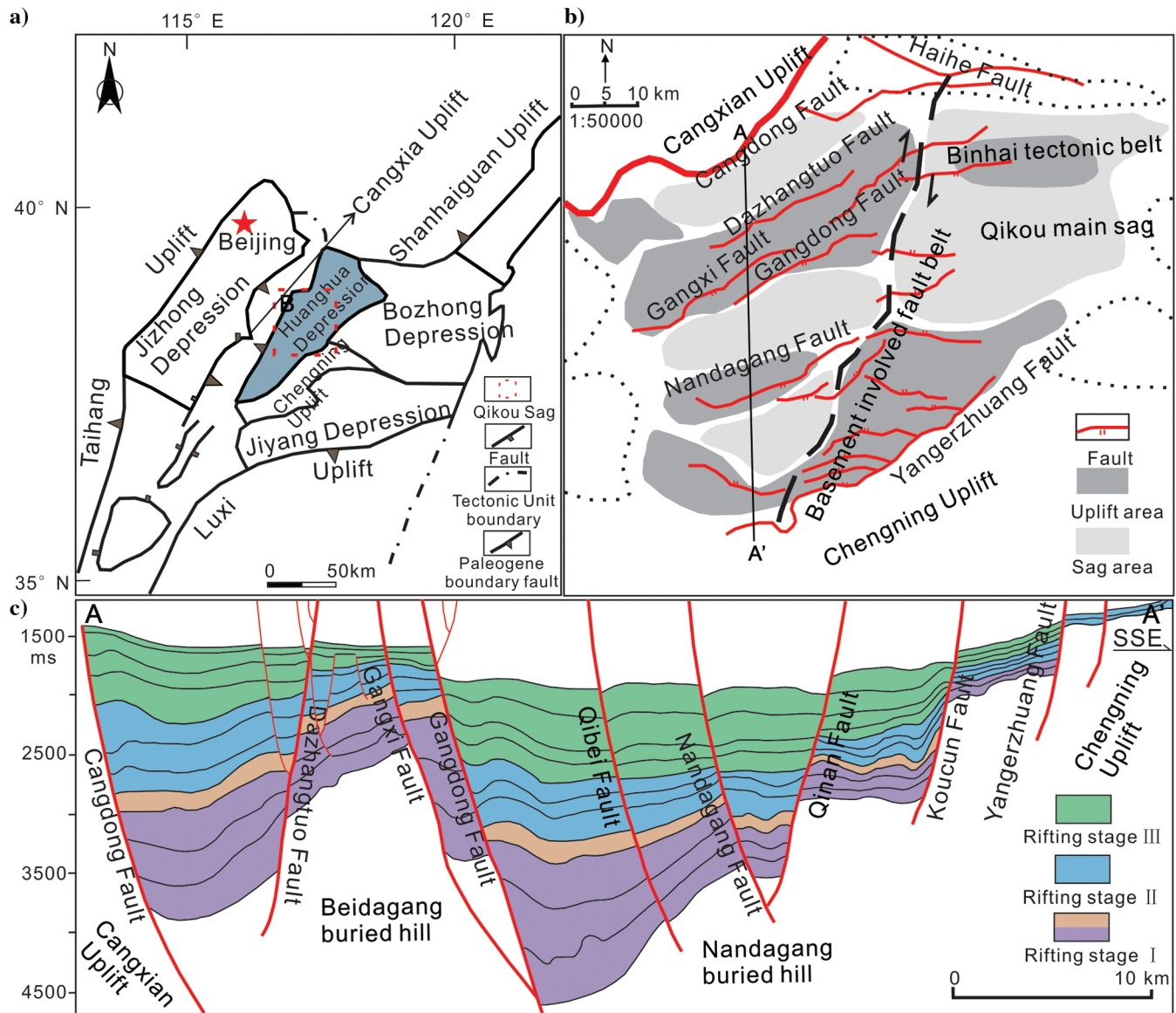


Figure 1. (a) Location of the study area in the Huanghua depression of eastern China (the red-dashed rectangle). (b) Nadagang uplift and the Nandagang fault within (c) the Shahejie Formation (lower green). The red lines are generalized faults, and not all faults are shown. Three main rifting stages are presented (adapted from Jiang et al., 2019).

Geologic setting

The Wangxuzhuang oilfield is located in the western part of the Bohai Bay Basin (Figure 1a; Jiang et al., 2019), in eastern China. It is a Cenozoic lacustrine basin formed upon the basement of the North China Craton. Our analyses use a 3D seismic survey from the Wangxuzhuang oilfield, covering the southern portion of the Nandagang fault zone (Figure 1b). The basin has experienced an active tectonic history, including: east–west striking granitic intrusions into the upper block of the Nandagang fault in the middle and late Proterozoic and the development of many northeast subsidiary faults due to the formation of the Luxi uplift and the Taihang mountains in the Cenozoic and Late Jurassic. The strata revealed by drilling the Wangxuzhuang oilfield from top to bottom are the Quaternary plain group, the Neocene (the Minghuazhen and Guantao Formations), the

Paleogene (the Dongying and Shahejie Formations), and the Mesozoic formations (Figure 1c). The Shahejie Formation is one of the primary hydrocarbon-bearing strata in this area. The lower Shahejie Formation (the first member) is approximately 200–600 m thick and consists of micritic limestone, calcareous shale, and argillaceous dolomite, which is different from the middle and upper members that are composed entirely of sandstone and mudstone. This study investigates the normal faults developed within the lower member of the Shahejie Formation at approximately 2–2.5 km in depth.

Methodology: Fault damage zone and seismic variance

A fault damage zone is composed of deformed rocks with reduced acoustic impedance compared to the undeformed host rock (protolith) (Chester and Logan, 1986; Caine et al., 1996). Permeability within the damage zone is intrinsically determined by the architecture and lithology of the host rock, the displacement along the fault, and any diagenetic reactions that occurred within it (Caine et al., 1996; Billi et al., 2003). The distribution of damage around a fault, and thus the damage zone itself, is often asymmetrical; e.g., the hanging-wall damage zone of normal faults (Figure 2) tends to be larger than the footwall damage zone. To detect the geometry of damage zones in the subsurface, we used the attribute of seismic variance with a window of –5 to +5 ms, which integrates the cumulative seismic effects caused by deformation (e.g., faults or fractures; Chopra and Marfurt, 2007; Iacopini and Butler, 2011; Liao et al., 2019). Variance (the opposite of coherence) is a measurement of the discontinuity of a seismic section. It is calculated in 3D and represents the trace-to-trace variability over a particular sample interval; therefore, it produces interpretable lateral changes in acoustic impedance. Similar traces produce low variance coefficients, whereas discontinuities have high variance coefficients (fractures/faults). The area of increased variance near the fault is regarded as the fault damage zone for the purpose of this study. As an analog to the intensity of fractures and structural discontinuities measured in outcrop, the high variance zone is interpreted as the fault core, the one-order wider zone of intermediate variance level is the damage zone, and the low variance zone is the country rock (the protolith zone) away from the fault. This approach (Liao et al., 2019) has been validated to conform with observations in field outcrops (Sagy et al., 2001; Mitchell and Faulkner, 2009; Savage and Brodsky, 2011).

Attribute results and analysis

Distribution of damage zones

The basin in this study is composed of a system of normal faults located on the upper block of the Nandagang fault (Figure 3). As observed in core samples and image logs, the distribution of fracture networks is considered a significant conduit for the migration of fluids on the basin scale (Yan et al., 2016). It is expected that

the damage zones around faults are densely fractured due to the uplift and bending of anticlinal formations (Reches, 1988; Staples, 2011) and associated stress localization around the secondary normal faults. We use the seismic attribute of variance, calculated from the 3D seismic reflection data, to image damage-zone widths, associated with faults in the Shahejie Formation.

Figure 3 shows the variance image computed from a patented algorithm. Significant observations include (1) distinguishable strips of high variance values in red-black, approximately trending east–west, parallel to the controlling Nandagang fault, (2) a few red-black strips trending north–south in the first block, (3) red-black patches scattering in the second and third blocks, and (4) large areas of low variance values in white-gray distributed throughout the map.

Thickness of damage zones

The red-black patches (Figure 3) are interpreted as structural discontinuities and are not the focus of this study. Comparatively, the white-gray area is relatively continuous, but with changes in seismic properties. The red-black strips are interpreted as normal fault damage zones that are systematically formed due to extension associated with Nandagang anticlinal folding (Figure 1b) during the Cenozoic and Late Jurassic. We picked six primary strips of normal faults (the red-black strips; Figure 3) in this study. For each strip, we prepared six vertical profiles of the seismic variance. The six profiles in each section display distribution of the seismic variance that we generalized as the characteristics of a normal fault damage zone. These sections reveal two groups of damage zones:

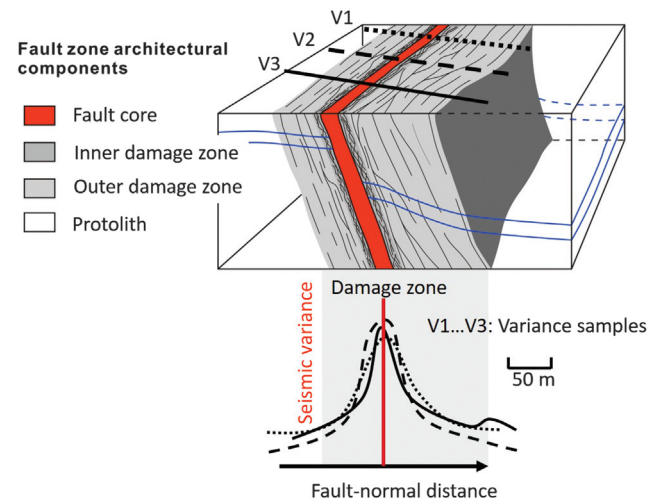


Figure 2. Conceptual models for the damage zone of a normal fault. Upper: schematic diagram showing the fault-zone architectural components. The red indicates the fault core, dark gray for the inner damage zone, gray for the outer damage zone, and the protolith is removed; seismic variance profiles are shown perpendicular to the fault. Lower: seismic variance profiles versus fault distance corresponding to the schematic fault zone.

- 1) Isolated normal faults: a typical damage zone with a well-developed single, central, fault core, represented by a zone of high variance, >0.6, and two zones of intermediate variance, 0.2–0.6 (gray in Figure 4), that decay to the background variance, 0–0.2 (Figure 4). The thicknesses of these damage zones range from 100 to 200 m. The fault lengths range from 1 to 3 km. The seismic variance pattern of faults 1–3 appears slightly asymmetrically, whereas fault 4 presents a strong asymmetrical shape.
- 2) Bifurcated faults: larger damage zones with a banded section of approximately 400–450 m thickness (Figure 5e and 5f). Fault 5 is approximately 3 km long and accompanied by a 1.5 km subfault, and fault 6 is composed of two approximately 1.3 km subfaults (trending north–south). These faults include different linked segments and several fault cores to be discussed later.

Synthesis of isolated faults

Previous studies of fault damage zones have used different methods to characterize fracture distribution for exposed faults. The mathematical modeling of fracture intensity decay with respect to the off-fault distance yields model fits that include log-normal, power-law, gamma, and exponential laws, among which the power-law distribution is the preferred model for damage zones (Savage and Brodsky, 2011; Liao et al., 2019). Figure 5 shows seismic variance (deformation) as a function of distance from the fault core for the aforementioned faults. We found that the variance value decay is well fit

by the power-law function: $y = ax^{-b}$, where y is the variance values, x is the distance from the fault core, b is an exponent describing the decay, and a is a constant that is fault-specific. Here, a and b are two constants that may reflect the physical properties related to the layer thickness or brittleness of the rock with slight differences. Such typical characteristics of the dimensions and shapes of the deformation zones in Figure 5a–5c (faults 1–3) are observed in the field cases (Vermilye and Scholz, 1998; Sagy et al., 2001; Mitchell and Faulkner, 2009). For high values of seismic variance in the fault core, the damage is likely related to intense damage in the form of gouge zones and pulverized rock in the fault core (Marone and Scholz, 1989). At great distances from the fault, the damage and fractures decrease to merge with the protolith values (Liao et al., 2019).

Discussion

Fault asymmetry and bifurcation

Fault asymmetry is commonly observed in the field. Berg and Skar (2005) uses outcrop data to examine the spatial arrangement of fractures in the damage zones of a segment of the large-scale Moab fault (45 km in length), southeast Utah. They find that the hanging-wall damage zone is more than three times wider than the footwall damage zone, and there was a higher abundance of antithetic fractures and deformation bands in the hanging wall than in the footwall. We do not observe such block differences for faults 1–3 in this study. The slight asymmetry might be associated with slight preferential rupture propagation that is commonly assumed

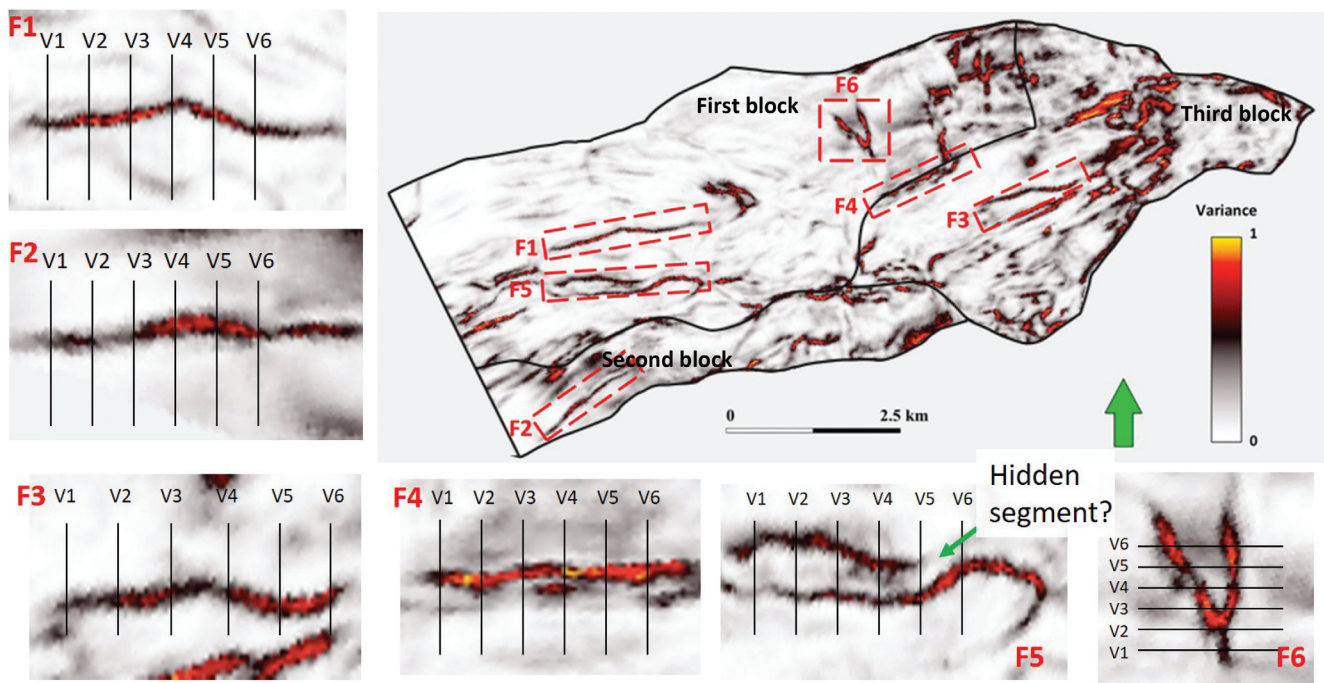


Figure 3. Map of the calculated variance of the 3D seismic survey in the lower member of the Shahejie Formation (the Nandagang uplift area in Figure 1B). This map is on the upper block of the Nandagang fault. Strips of variance attribute within the red boxes are secondary faults with magnified maps. F1, fault 1; F2, fault 2; F3, fault 3; F4, fault 4; F5, fault 5; and F6, fault 6.

along normal faults (Ben-Zion and Shi, 2005; Ampuero and Mao, 2017).

Another possibility is that fault asymmetry is a consequence of structures associated with multiple secondary faults (Aydin and Johnson, 1978). Such secondary discontinuities impact the seismic variance values, as observed in the aforementioned faults. As such, the more damaged blocks are expected to have more secondary structures. It is suggested that the damage zones of faults 4–6 are formed by the superposition of several subfaults.

We examine each profile of the faults 5 and 6 that clearly present systems of fault bifurcations relating to such subfaults. Two simple idealized systems are discussed here: a merged system and a bifurcated system. For both systems, each profile of seismic variance perpendicular to the fault shows the internal structural components at a specific location. The in-

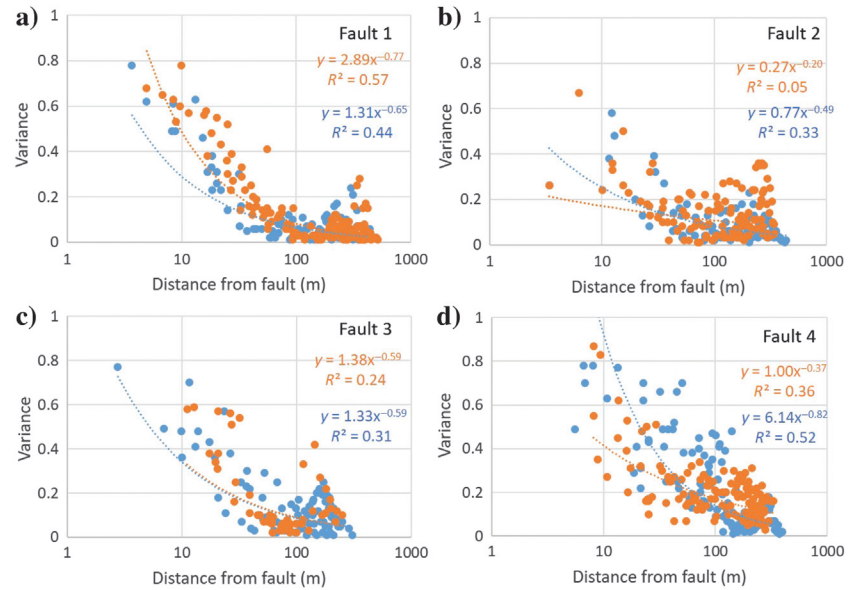


Figure 5. Seismic variance as a function of the fault distance from the fault. All data (F1–F4) are well fit by the model $= ax^{-b}$, where coefficients a and b are fault related. Orange is the hanging wall, and blue is the footwall.

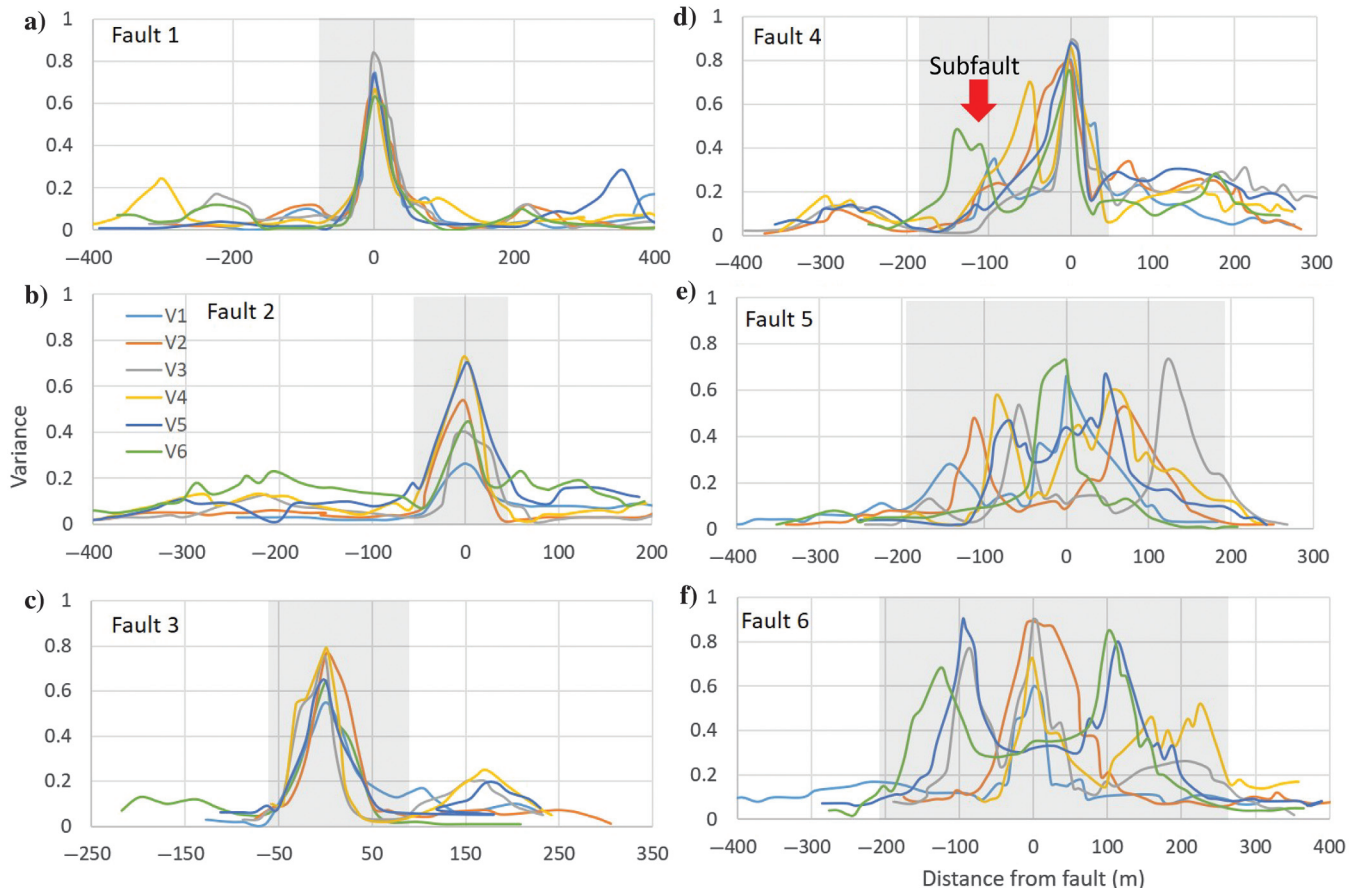


Figure 4. Profiles of the seismic variance values across the damage zones of selected normal faults; profiles locations in Figure 3; variance values above the background are interpreted as damage zones. Isolated faults: F1, F2, F3, and F4; Bifurcated faults: F5 and F6. Note the variance asymmetry of fault 4 that is associated with a subsidiary fault.

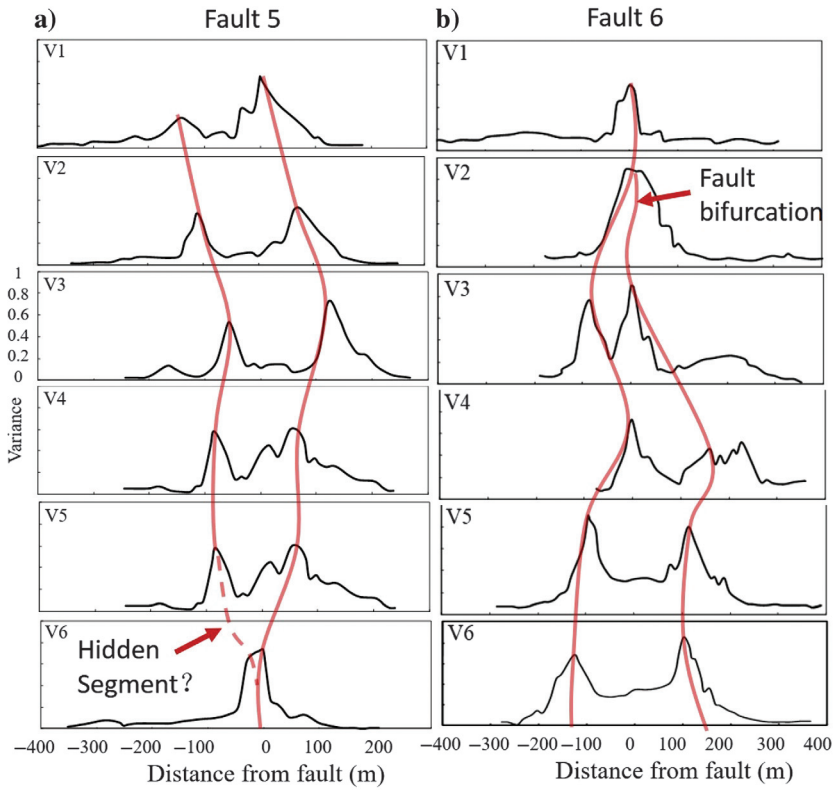


Figure 6. Attribute variations of damage zones along with strike intervals. (a) A merged fault (fault 5) with one hidden segment. (b) A bifurcated fault (fault 6) with two subsegments. Note that the variance value between the pulses is higher than background values, which indicates the superposition effect of the two subsegments.

terpreted damage zones in fault 5 are shown by two connected red lines in Figure 6a. From V1 to V5, one small damage zone (the left one with lower variance values) and a large one (the right one with a higher value) are recognizable with two peaks of seismic variances. These two peaks merged with each other in profile V6. The variance values between the two peaks illustrate an overprinted increase, which reveals the increasing deformation of the mixed zone heterogeneity when the two faults merge. The profile of V6 becomes a typical peak of seismic variance for an isolated fault. For the missing variance strip in Figure 3 (the green arrow in fault 5), we proposed a hidden (subseismic) fault segment with little displacement between profiles of V5 and V6. In the case of little fault displacement, the seismic attribute of variance is not sensitive enough to detect the discontinuity.

Fault 6 in Figure 3 is treated as a bifurcated system. Profile of V2 in Figure 6b illustrates the exaggeration of seismic variances before being bifurcated into two faults in the profile of V3. The seismic variances express the interacting deformation of the two damage zones of subfaults. The damage-zones' thickness is approximately 400 m composed of overprinted bifurcated segments. This cumulative effect is expected to disappear if the spaced distance between the two bifurcated segments is larger than the thickness of an isolated fault.

Fault length and fault displacement

To investigate the relationship between the total fault length and displacement, we combined our results with published displacement-length (D-L) profiles (Figure 7). Assuming that the limestone velocity is 3.5 km/s, we calculated the displacements for faults 1–4 by multiplying the time differences between fault blocks from the 3D seismic data (Table 1). Figure 7 shows that the amount of displacement on a fault is proportional to the fault length. Our data (the green dots) of these four faults fit well into such a general relation; however, the displacements increase at a faster rate in this study. Jackson and Rovetan (2013) propose two stages of D-L growth paths for normal faults: The first stage is lengthening rapidly with various displacements, e.g., tip propagation, relay formation, and breakdown, segment linkage etc.; The second stage is large displacement without much fault lengthening, e.g., subvertical constant-length growth. In this study, it is likely that the growth of normal faults in limestone demonstrates characteristics mostly in the second stage. Additionally, most normal faults in this study grow with damage zones of approximately 200 m width, irrespective of the fault displacement and length,

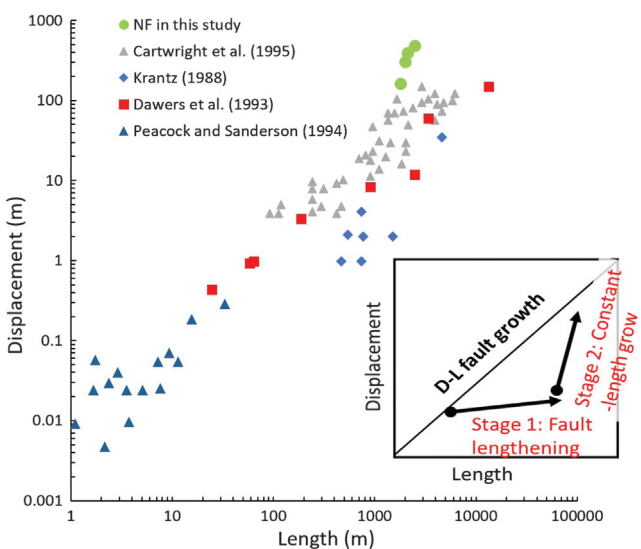


Figure 7. Displacement versus length for normal faults plotted in log-log scales (NF, normal fault; NF data are extracted from Krantz, 1988; Dawers et al., 1993; Peacock and Sanderson, 1994; Cartwright et al., 1995). The inset is a schematic model for the two stages of fault growth. Stage 1, fault lengthening with various displacement and Stage 2, constant-length growth.

Table 1. Parameters of fault geometries.

Displacement in time (ms)	Length (km)	Hanging wall		Footwall		
		a	b	a	b	
Fault 1	131	2.5	2.89	0.77	1.31	0.65
Fault 2	104	2.1	0.27	0.2	0.77	0.49
Fault 3	35	1.8	1.38	0.59	1.33	0.59
Fault 4	65	2.0	1	0.37	6.41	0.82

which we tentatively argue as being potentially a result of the systematic and abrupt deformation and the brittleness of limestone.

Reservoir compartmentalization and fluid flow

Figure 3 demonstrates that the distribution of deformation (the red strips and patches) in limestone is highly heterogeneous spatially. The fault damage zones (the red strips) are expected to provide high fault-parallel permeability pathways to transport fluids. Nevertheless, **3** most hydrocarbon traps in this study have been found near the damage zones. Estimation of the fault-zone permeability is difficult because faults usually are avoided by borehole drilling. The observation of tracer trajectories in boreholes indicates the significant channeling of flow within the damage zones along the fault strike. The favored flow direction can be explained by the macroscale fracture networks within the damage zones. We inferred that the variation of permeability exists horizontally because we found fault-bounded hydrocarbon traps. The fault sealing is due to gouge accumulation in the fault cores, which may lead to the compartmentalization of the basin. Thus, the spatial distribution of the fault system is a highly interrelated approach to understand the fluid flow in the subsurface.

Conclusion

In this study, we display an approach to apply seismic variance to characterize the structure and distribution of a system of normal faults in eastern China. We have demonstrated characteristics of the damage zones and within limestone in the subsurface, and we recognize four isolated faults of approximately 200 m damage-zone thickness and two bifurcated faults of approximately 400 m thickness. We infer that the overprinting of faults and rupture preference leads to the structure asymmetry. This approach and these data present the potential for evaluating fault damage zones on a regional scale that impacts the migration and accumulations of petroleum.

Acknowledgments

The authors would like to thank the reviewers and S. Chen. We also thank PetroChina (data license), Petrel, and AASPI at the University of Oklahoma. Partial funding was provided by Chinese National Science and Technology Major Project 2016ZX05024-003-008.

Data and materials availability

Data associated with this research are available and can be obtained by contacting the corresponding author.

References

- Ampuero, J. P., and X. Mao, 2017, Upper limit on damage zone thickness controlled by seismogenic depth, in M. Y. Thomas, T. M. Mitchell, and H. S. Bhat, eds., *Geophysical Monograph Series*, **216**, doi: [10.1007/BF00876547](https://doi.org/10.1007/BF00876547).
- Aydin, A., and A. M. Johnson, 1978, Development of faults as zones of deformation bands and as slip surfaces in sandstone: Pure and Applied Geophysics, **116**, 931–942, doi: [10.1007/BF00876547](https://doi.org/10.1007/BF00876547).
- Ben-Zion, Y., and Z. Shi, 2005, Dynamic rupture on a material interface with spontaneous generation of plastic strain in the bulk: Earth and Planetary Science Letters, **236**, 486–496, doi: [10.1016/j.epsl.2005.03.025](https://doi.org/10.1016/j.epsl.2005.03.025).
- Berg, S. S., and T. Skar, 2005, Controls on damage zone asymmetry of a normal fault zone: Outcrop analyses of a segment of the Moab fault, SE Utah: Journal of Structural Geology, **27**, 1803–1822, doi: [10.1016/j.jsg.2005.04.012](https://doi.org/10.1016/j.jsg.2005.04.012).
- Billi, A., F. Salvini, and F. Storti, 2003, The damage zone-fault core transition in carbonate rocks: Implications for fault growth, structure and permeability: Journal of Structural Geology, **25**, 1779–1794, doi: [10.1016/S0191-8141\(03\)00037-3](https://doi.org/10.1016/S0191-8141(03)00037-3).
- Botter, C., N. Cardozo, S. Hardy, I. Lecomte, G. Paton, and A. Escalona, 2016, Seismic characterization of fault damage in 3D using mechanical and seismic modeling: Marine and Petroleum Geology, **77**, 973–990, doi: [10.1016/j.marpetgeo.2016.08.002](https://doi.org/10.1016/j.marpetgeo.2016.08.002).
- Busetti, S., K. Mish, P. Hennings, and Z. Reches, 2012, Damage and plastic deformation of reservoir rocks—Part 2: Propagation of a hydraulic fracture: AAPG Bulletin, **96**, 1711–1732, doi: [10.1306/02011211011](https://doi.org/10.1306/02011211011).
- Caine, J. S., J. P. Evans, and C. B. Forster, 1996, Fault zone architecture and permeability structure: Geology, **24**, 1025–1028, doi: [10.1130/0091-7613\(1996\)024<1025:FZAAPS>2.3.CO;2](https://doi.org/10.1130/0091-7613(1996)024<1025:FZAAPS>2.3.CO;2).
- Cartwright, J. A., B. D. Trudgill, and C. S. Mansfield, 1995, Fault growth by segment linkage: An explanation for scatter in maximum displacement and trace length data from the Canyonlands Grabens of SE Utah: Journal of Structural Geology, **17**, 1319–1326, doi: [10.1016/0191-8141\(95\)00033-A](https://doi.org/10.1016/0191-8141(95)00033-A).
- Chester, F. M., and J. M. Logan, 1986, Implications for mechanical properties of brittle faults from observations of the Punchbowl fault zone, California: Pure and Applied Geophysics, **124**, 79–106, doi: [10.1007/BF00875720](https://doi.org/10.1007/BF00875720).
- Chopra, S., and K. J. Marfurt, 2007, Seismic attributes for prospect identification and reservoir characterization: SEG, SEG Geophysical Developments Series, No. 11, doi: [10.1190/1.9781560801900](https://doi.org/10.1190/1.9781560801900).
- Dawers, N. H., M. H. Anders, and C. H. Scholz, 1993, Growth of normal faults: Displacement-length scaling:

- Geology, **21**, 1107–1110, doi: [10.1130/0091-7613\(1993\)021<1107:GONFDL>2.3.CO;2](https://doi.org/10.1130/0091-7613(1993)021<1107:GONFDL>2.3.CO;2).
- Ellis, M. A., S. E. Laubach, P. Eichhubl, J. E. Olson, and P. Hargrove, 2012, Fracture development and diagenesis of Torridon Group Applecross Formation, near An Teallach, NW Scotland: Millennia of brittle deformation resilience: *Journal of Geological Society*, **169**, 297–310, doi: [10.1144/0016-76492011-086](https://doi.org/10.1144/0016-76492011-086).
- Faulkner, D. R., C. A. L. Jackson, R. J. Lunn, R. W. Schliesche, Z. K. Shipton, C. A. J. Wibberley, and M. O. Withjack, 2010, A review of recent developments concerning the structure, mechanics and fluid flow properties of fault zones: *Journal of Structural Geology*, **32**, 1557–1575, doi: [10.1016/j.jsg.2010.06.009](https://doi.org/10.1016/j.jsg.2010.06.009).
- Iacopini, D., and R. W. H. Butler, 2011, Imaging deformation in submarine thrust belts using seismic attributes: *Earth and Planetary Science Letters*, **302**, 414–422, doi: [10.1016/j.epsl.2010.12.041](https://doi.org/10.1016/j.epsl.2010.12.041).
- Jackson, C. A. L., and A. Rotevatn, 2013, 3D seismic analysis of the structure and evolution of a salt-influenced normal fault zone: A test of competing fault growth models: *Journal of Structural Geology*, **54**, 215–234, doi: [10.1016/j.jsg.2013.06.012](https://doi.org/10.1016/j.jsg.2013.06.012).
- Jiang, S., W. Wang, A. Zhang, and W. Zhou, 2019, Genetic mechanism and evolution of the covert fault zone and its oil-controlling mode in Qikou Sag, eastern China: *Energies*, **12**, 98, doi: [10.3390/en12010098](https://doi.org/10.3390/en12010098).
- Katz, O., Z. Reches, and G. Baer, 2003, Faults and their associated host rock deformation — Part 1: Structure of small faults in a quartz–syenite body, southern Israel: *Journal of Structural Geology*, **25**, 1675–1689, doi: [10.1016/S0191-8141\(03\)00011-7](https://doi.org/10.1016/S0191-8141(03)00011-7).
- Krantz, R. W., 1988, Multiple fault sets and three dimensional strain: Theory and application: *Journal of Structural Geology*, **10**, 225–237, doi: [10.1016/0191-8141\(88\)90056-9](https://doi.org/10.1016/0191-8141(88)90056-9).
- Laubach, S. E., P. Eichhubl, P. Hargrove, M. A. Ellis, and J. N. Hooker, 2014, Fault core and damage zone fracture attributes vary along strike owing to interaction of fracture growth, quartz accumulation, and differing sandstone composition: *Journal of Structural Geology*, **68**, 207–226, doi: [10.1016/j.jsg.2014.08.007](https://doi.org/10.1016/j.jsg.2014.08.007).
- Liao, Z., H. Liu, B. M. Carpenter, K. J. Marfurt, and Z. Reches, 2019, Analysis of fault damage-zones by using 3D seismic coherence in Anadarko Basin, Oklahoma: AAPG Bulletin, **103**, 1771–1785, doi: [10.1306/1219181413417207](https://doi.org/10.1306/1219181413417207).
- Liao, Z., H. Liu, Z. Jiang, K. J. Marfurt, and Z. Reches, 2017, Fault damage zone at subsurface: A case study using 3D seismic attributes and a clay model analog for the Anadarko Basin, Oklahoma: *Interpretation*, **5**, T143–T150, doi: [10.1190/INT-2016-0033.1](https://doi.org/10.1190/INT-2016-0033.1).
- Marone, C., and C. H. Scholz, 1989, Particle-size distribution and microstructure within simulated fault gouge: *Journal of Structural Geology*, **11**, 799–814, doi: [10.1016/0191-8141\(89\)90099-0](https://doi.org/10.1016/0191-8141(89)90099-0).
- Mitchell, T. M., and D. R. Faulkner, 2009, The nature and origin of off fault damage surrounding strike-slip fault zones with a wide range of displacements: A field study from the Atacama fault system, northern Chile: *Journal of Structural Geology*, **31**, 802–816, doi: [10.1016/j.jsg.2009.05.002](https://doi.org/10.1016/j.jsg.2009.05.002).
- Peacock, D. C. P., and D. J. Sanderson, 1994, Geometry and development of relay ramps in normal fault systems: AAPG Bulletin, **78**, 147–165, doi: [10.1306/BDF90461718-11D7-8645000102C1865D](https://doi.org/10.1306/BDF90461718-11D7-8645000102C1865D).
- Peng, Z., Y. Ben-Zion, A. J. Michael, and L. Zhu, 2003, Quantitative analysis of seismic fault zone waves in the rupture zone of the 1992 Landers, California, earthquake: Evidence for a shallow trapping structure: *Geophysical Journal International*, **155**, 1021–1041, doi: [10.1111/j.1365-246X.2003.02109.x](https://doi.org/10.1111/j.1365-246X.2003.02109.x).
- Pigott, J. D., M. H. Kang, and H. C. Han, 2013, First order seismic attributes for clastic seismic facies interpretation: Examples from the East China Sea: *Journal of Asian Earth Sciences*, **66**, 34–54, doi: [10.1016/j.jseaes.2012.11.043](https://doi.org/10.1016/j.jseaes.2012.11.043).
- Reches, Z., 1988, Evolution of fault patterns in clay experiments: *Tectonophysics*, **145**, 141–156, doi: [10.1016/0040-1951\(88\)90322-8](https://doi.org/10.1016/0040-1951(88)90322-8).
- Rossetti, F., L. Aldega, F. Trcce, F. Balsamo, A. Billi, and M. Brilli, 2010, Fluid flow within the damage zone of the Boccheggiano extensional fault (Larderello–Travale geothermal field, central Italy): Structures, alteration and implications for hydrothermal mineralization in extensional settings: *Geological Magazine*, **148**, 558–579, doi: [10.1017/S001675681000097X](https://doi.org/10.1017/S001675681000097X).
- Sagy, A., Z. Reches, and I. Roman, 2001, Dynamic fracturing: Field and experimental observations: *Journal of Structural Geology*, **23**, 1223–1239, doi: [10.1016/S0191-8141\(00\)00190-5](https://doi.org/10.1016/S0191-8141(00)00190-5).
- Savage, H. M., and E. E. Brodsky, 2011, Collateral damage: Evolution with displacement of fracture distribution and secondary fault strands in fault damage zones: *Journal of Geophysical Research*, **116**, B03405, doi: [10.1029/2010JB007665](https://doi.org/10.1029/2010JB007665).
- Staples, E., 2011, Subsurface and experimental analyses of fractures and curvature: M.S. thesis, University of Oklahoma.
- Vermilye, J. M., and C. H. Scholz, 1998, The process zone: A microstructural view of fault growth: *Journal of Geophysical Research*, **103**, 12223–12237, doi: [10.1029/98JB00957](https://doi.org/10.1029/98JB00957).
- Yan, R., L. Zeng, X. Zhao, Z. Liao, and M. Chen, 2016, Fracture development characteristics and its formation mechanism in Lower Member 1 Shahejie biolithite reservoir, Z oilfield, Bohai Bay (in Chinese with English abstract): *Chinese Journal of Geology*, **51**, 484–493.
- Zoback, M. D., S. Hickman, and W. Ellsworth, and the SAFOD Science Team, 2011, Scientific drilling into the San Andreas fault zone — An overview of SAFOD's first five years: *Scientific Drilling*, **11**, 14–28, doi: [10.5194/sd-11-14-2011](https://doi.org/10.5194/sd-11-14-2011).

Biographies and photographs of authors are not available.